IRON OXIDE NANOPARTICLES SYNTHESIS, SURFACE MODIFICATION, CHARACTERIZATION AND ITS TOXICITY ASSAY

S. Glory Sobha[1,2], Ambrose Rejo Jeice[2*], S. Ilangovan[1]

[1]*P.G and Research Department of Physics, Thiru Vi Ka Government Arts College, Thiruvarur (Affiliated to Bharathidasan University, Tiruchirappalli, Tamil Nadu 620023)*

[2]*Department of Physics* & Research Centre, *Annai Velankanni College, Tholayavattam 629157, Kanyakumari District, Tamil Nadu, India-629157*

**Corresponding* author: Ambrose Rejo Jeice (rejojeice@gmail.com)

Mobile No : +918807841121

Abstract

The aim of the research work is to produce iron oxide nanoparticles (NPs) and modify their surface to reduce their toxicity. The iron oxide NPs were synthesized using the chemical co-precipitation process, and studied the UV-Vis, SEM, XRD, DLS, Zeta analyzer and FTIR spectroscopes. *Bacillus subtilis* and *Escherichia coli* were used as test organisms for assessing the harmfulness of iron oxide NPs and amended iron oxide NPs. It was concluded that iron oxide NPs have harmfulness towards these test organisms at higher concentrations, whereas amended iron oxide NPs do not have this property. The research supports the idea that surface redesign with biocompatible substances like chitosan can reduce the toxicity of NPs.

Key words: UV-Vis, Zeta analyzer, Iron chloride tetra hydrate, XRD and FTIR spectroscopes.

1. INTRODUCTION

NPs have diameters between 1 and 100 nm. A NP is, in theory, any group of atoms that are bound together and have a structural measure smaller than 100 nm. They serve just as a bridge between atomic or molecular structures and bulk materials. In comparison to bulk materials, NPs exhibit various chemical and physical characteristics, namely lower melting temperatures, unique magnetizations greater surface areas, mechanical strength and unique optical characteristics [1-4]. Surface and interfacial characteristics can change in the presence of chemical substances. Such substances can indirectly stabilize in opposition to coagulation and aggregation by retaining particle charge and altering the particle's outermost layer.

Iron oxide NPs production has seen extensive development over the last 10 years, not only for its core scientific interest but also for a wide range of technological and medicinal applications [5-7]. Iron oxide NPs have attracted a lot of attention due to a variety of features, including their super paramagnetic nature, strong force, low Curie temperature, high magnetic susceptibility, etc. [8-10]. When iron oxide NPs are released into the environment, they frequently interact with air, water, and soil and affect the surface properties of the particles, which might cause particle aggregation or other surface property changes [11]. These non-biodegradable NPs are being given various surface changes to make them more biocompatible. To achieve combined properties of high magnetic saturation, biocompatibility, and interactive functions on the surface, the iron oxide NPs need to be pre-coated with chitosan, a biopolymer, which increases their stability, biodegradability, and non-toxicity in the physiological medium [12]. We still don't fully understand how NPs and living systems interact. We must investigate the antibacterial activity of both iron oxide NPs and modified iron oxide NPs in order to comprehend the interaction mechanism.

2. MATERIAL AND METHODS

2.1 Materials

From Sigma-Aldrich, anhydrous ferric chloride ($FeCl_3$, 99%), ferrous chloride ($FeCl_2$, 99%), ethanol, acetone, hydrochloric acid, ammonia solution 30% (NH_4OH) (India) and chitosan were obtained. Analytical-grade chemicals were employed throughout. The pathogenic *Bacillus subtilis* (MTCC 7164) and *E. coli* (MTCC 1089) used in the study were obtained from Institute of Microbial Technology, Chandigarh.

2.2 Synthesis of iron oxide NPs

The co-precipitation of iron chloride tetrahydrate ($FeCl_2.4H_2O$) and iron chloride hexahydrate ($FeCl_3.6H_2O$) produced the iron oxide NPs. In 100 ml of deionized water, solutions of iron chloride tetrahydrate ($FeCl_2.4H_2O$) and iron chloride hexahydrate ($FeCl_3.6H_2O$) were made while maintaining molar concentrations of 0.1M and 0.2M, respectively. To form a homogeneous solution, the solution was combined in a beaker and then swirled using a magnetic stirrer. The solution was sealed and heated in a water bath for 15 to 20 minutes at 60^oC. To the initial solution, 14 ml of sodium hydroxide (NaOH) were then added. After the reaction was completed, a dark precipitate was formed. After 15 minutes of centrifugation at 7000 rpm, the precipitate was collected as a pellet. Iron oxide NPs were then obtained in powder form by drying the pellet at a temperature of 50 C.

2.3 Surface modification of synthesized iron oxide NPs

Iron oxide NPs can have their surface properties improved through surface modification. Iron oxide NPs' compatibility with the biological environment, stability in suspensions, and ability to resist aggregation are all improved through surface modification. Chitosan was dissolved in 100 cc of 1 M acetic acid for the purpose of surface modification. Then it was thoroughly mixed using a magnetic stirrer for 15 minutes, after which 20 grams of chitosan were added, and it was swirled for 30 minutes. Then 70 mg of iron oxide NPs was added, and the magnetic stirrer was used to mix the solution for 18 hours. The result was a uniform dark brown suspension. The sample was centrifuged at 7000 rpm for 15 minutes and after 18 hours; the pellets were collected, which was then dried in a hot air oven.

2.4 Characterization

Iron oxide NPs and surface modified iron oxide NPs were then obtained in powder form by drying the pellet at a temperature of 50^oC and the results were qualitatively examined using Perkin Elmer Lambda (Model EZ-221) UV-visible spectroscopy (wavelength 200- 800 nm). DLS analyser was used to estimate the particle size of the iron oxide and chitosan modified iron oxide NPs. Malvern Nano ZS (Zetasizer Nano Series, Worcestershire, UK) was used to estimate zeta potential of the iron oxide and chitosan modified iron oxide NPs, while they were dispersed in distilled water with a conductivity of 50 S/cm (arranged to by NaCl). The particle size of NPs was calculated after the particles were mixed in distilled water. Cu Kα radiation with an approximate wavelength

of 1.54 Å was used to perform the X-ray diffraction in order to confirm the phases of iron oxide NP (Shimadzhu 7000). When operating at 40 mA and 40 kV, continuous scan XRD data were obtained at diffraction angles between 20° and 80°. Using the Scherrer approximation, peak broadening was calculated from the full-width at half maximum (FWHM). Step scan was carried out. Maximum deconvolution, and Shimadzu's X-ray diffractometer was used to measure lattice parameters. The XRD was included with the XD-D1 software. The patterns of X-ray diffraction from the Maghemite and magnetite were found to overlap in JCPDS 19-629 and 39-1346. Fourier Transform Infrared Spectroscopy was used to analyse the identification and phase of the element for magnetite NP (Perkin Elmer version 10.03.07). Using a Perkin Elmer FTIR 1620 Fourier transform infrared spectrophotometer, infrared spectroscopy (FT-IR) was carried out between 400 and 4000 cm^{-1}. Using the nanosight NPs tracking system analyser, the hydrodynamic diameter of the NPs in the colloidal suspensions was measured. For each sample, about 400 measurements were processed to produce statistically meaningful results. The morphology, size, and chemical composition of individual NPs were examined using a field emission gun scanning electron microscope (JEOL JSM-7600F FEG-SEM) fitted with energy dispersive X-ray analysis (EDX) [13].

2.5 Toxicity study

The organisms were kept on nutrient agar slopes at 4 °C and subcultured before use. The absorption of iron oxide NPs and chitosan coated iron oxide NP suspensions in the presence of test organisms *E. coli* and *B. subtilis* were determined at a wavelength of 600 nm using UV visible Spectrophotometer and the growth kinetics was studied. Colony image analysis of *E. coli* and *B. subtilis* in the presence of iron oxide and chitosan coated iron oxide NPs were carried out using phase microscopy[14].

3 RESULTS AND DISCUSSION

3.1 Synthesis of iron oxide NPs

Iron oxide NPs developed using the chemical precipitation process is depicted in Fig 1(a). The colour of produced NPs in powder form is black. The modified Iron oxide NPs are depicted in Fig.1(b) and were synthesized using the biocompatible polymer chitosan. The colour of the chitosan solution changes to brown when iron oxide NP is added.

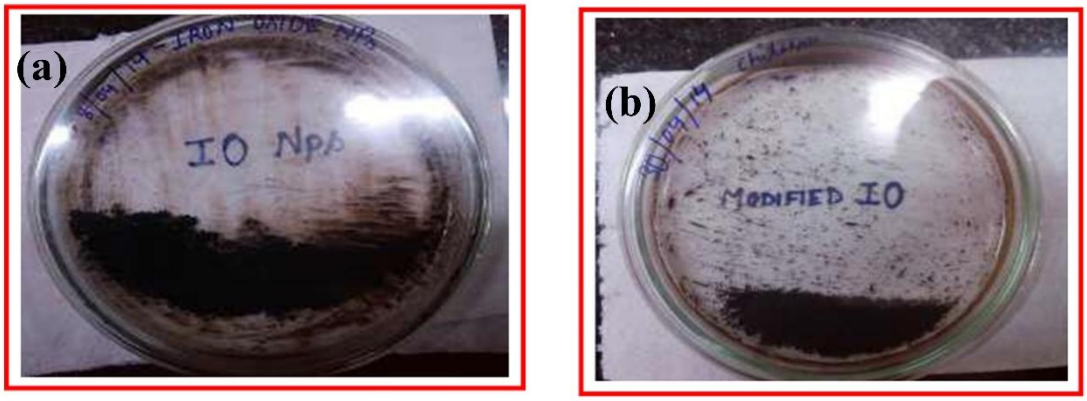

Fig.1(a) Chemically synthesized Iron oxide NPs (b) Chitosan modified Iron oxide NPs

3.2 UV-Visible Spectroscopy

Fig. 2 displays the UV-Visible spectra of iron oxide NPs and iron oxide NPs treated with chitosan. While chitosan-modified iron oxide NPs have a peak at 268 nm, iron oxide NPs exhibit a peak at 222 nm. Peak shifting proves that chitosan has been applied to the surface of iron oxide NPs [15].

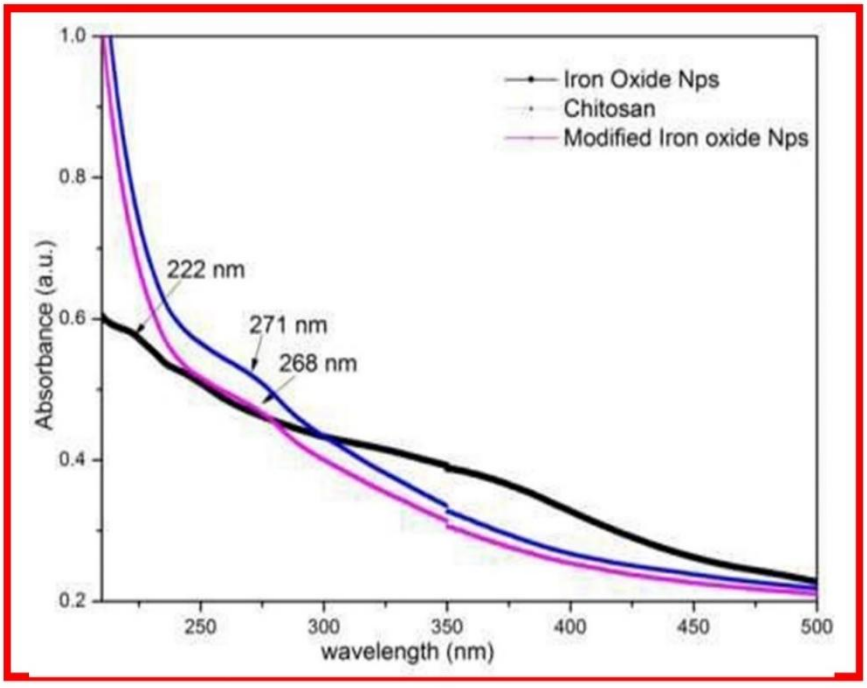

Fig. 2 UV spectrum of chitosan, Iron oxide and modified Iron oxide NPs

3.3 DLS analysis

Fig. 3(a) and 3(b) depicts the particle size distribution of iron oxide NPs and chitosan modified iron oxide NPs synthesized chemically. Iron oxide NPs are typically 104 nm in size, while chitosan-modified iron oxide NPs are typically 157 nm in size [16].

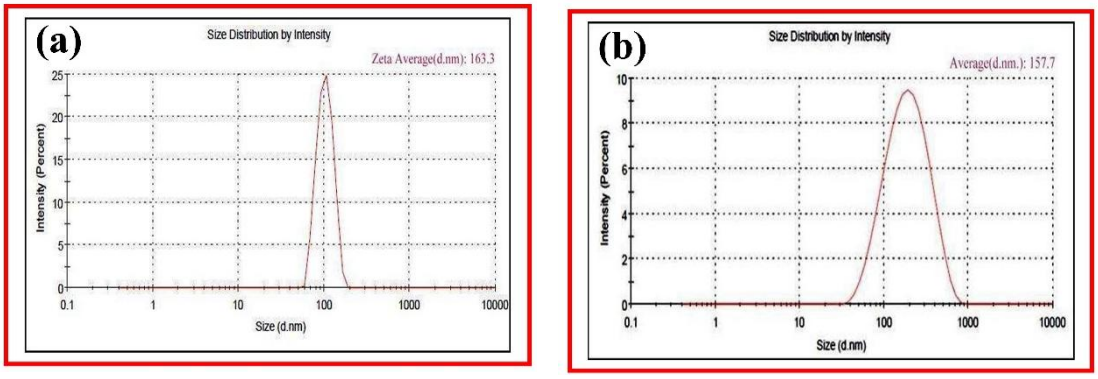

Fig. 3(a) Particle size distribution of Iron oxide NPs and Fig. 3(b) Particle size distribution of modified Iron oxide NPs

3.4 Zeta potential analysis

The zeta potential is the potential difference between the stationary fluid layer adhering to the dispersed particle and the dispersion medium. Zeta potentials for iron oxide NPs and iron oxide NPs treated with chitosan are shown in Fig. 4(a) and 4(b). Iron oxide NPs have a zeta potential of -32.2 mV, but chitosan-modified iron oxide NPs have a zeta potential of 36 mV. Chitosan-modified iron oxide NPs are more stable than iron oxide NPs, as evidenced by their greater zeta potential values [17]. The investigation demonstrates that adding chitosan to the iron oxide NPs surface boosts stability.

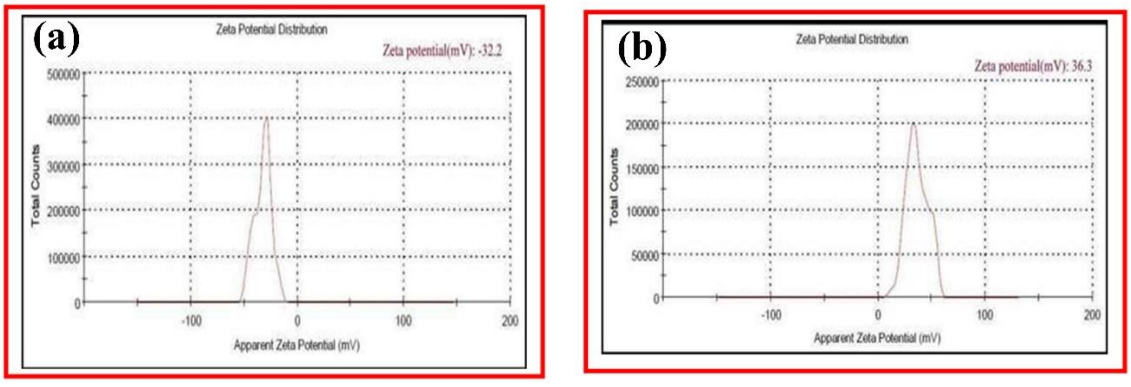

Fig. 4(a) Zeta potential of Iron oxide NPs and Fig. 4(b) Zeta potential of modified Iron oxide NPs

3.5 XRD analysis

Iron oxide NPs XRD pattern is displayed in Fig. 5. The crystalline structure of the iron oxide NPs is confirmed by the narrow peaks in the picture [18]. From the XRD pattern, the lattice spacing calculated from the diffraction peaks matched the [220], [311], [222] and [311] planes of Iron oxide NPs.

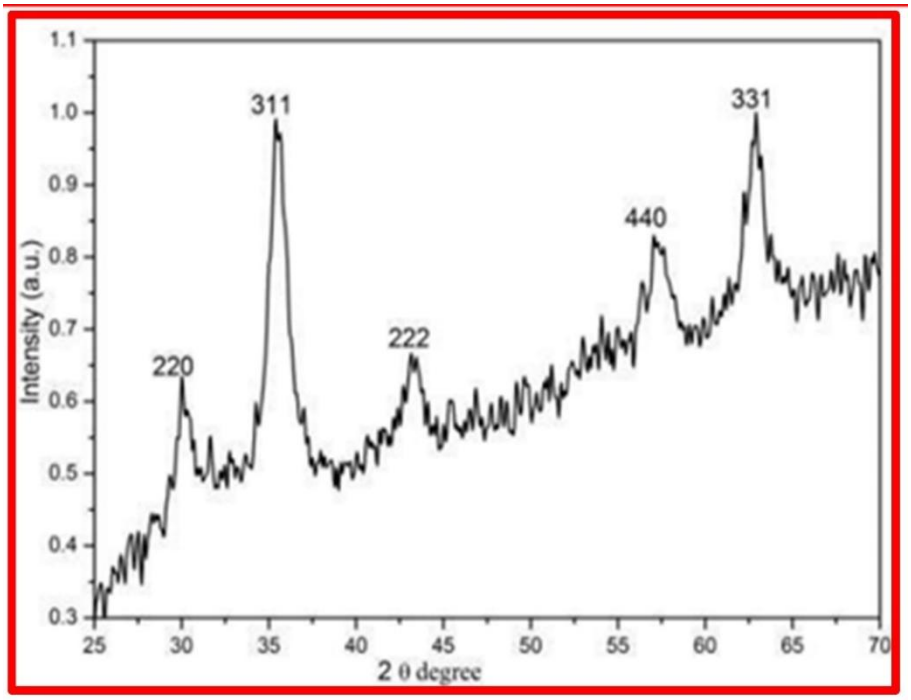

Fig. 5 XRD pattern of Iron oxide NPs

3.6 FTIR analysis

The FTIR spectra for iron oxide and modified iron oxide NPs are displayed in Fig. 6. The existence of NPs in the synthesized samples and surface-modified samples is confirmed by the peaks at 519 cm^{-1} and 514 cm^{-1}. The hydrogen interaction between the oxygen molecule in the iron oxide NPs and the hydrogen molecule in the chitosan indicates that the amide-I vibration for chitosan is about 1676 cm^{-1}, while for modified iron oxide NPs it

is moved to 1708 cm^{-1}. The coating of chitosan on the surface of iron oxide NPs is further supported by an FTIR investigation [19].

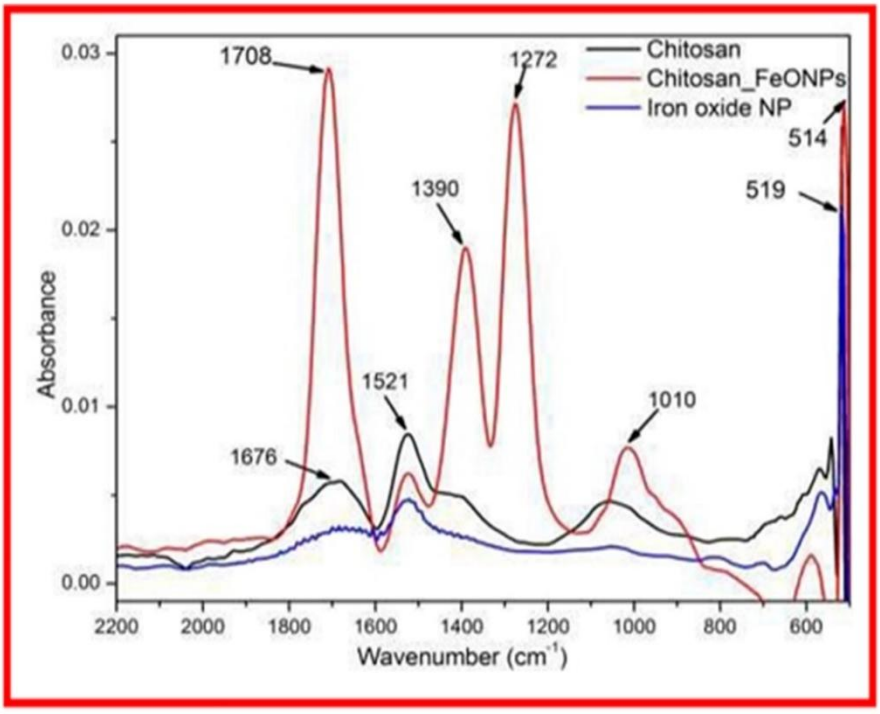

Fig.6 FTIR of chitosan, Iron oxide and modified Iron oxide NPs

3.7 SEM analysis

Iron oxide NPs produced using the chemical precipitation method is depicted in Fig. 7(a) whereas modified Iron oxide NP is depicted in Fig.7(b). The size of the particles in iron oxide NPs ranges from 8 to 20 nm, and it ranges from 15 to 25 nm for surface-modified iron oxide NPs. The NPs' increase in size is proof that chitosan was used to coat the iron oxide NPs [20].

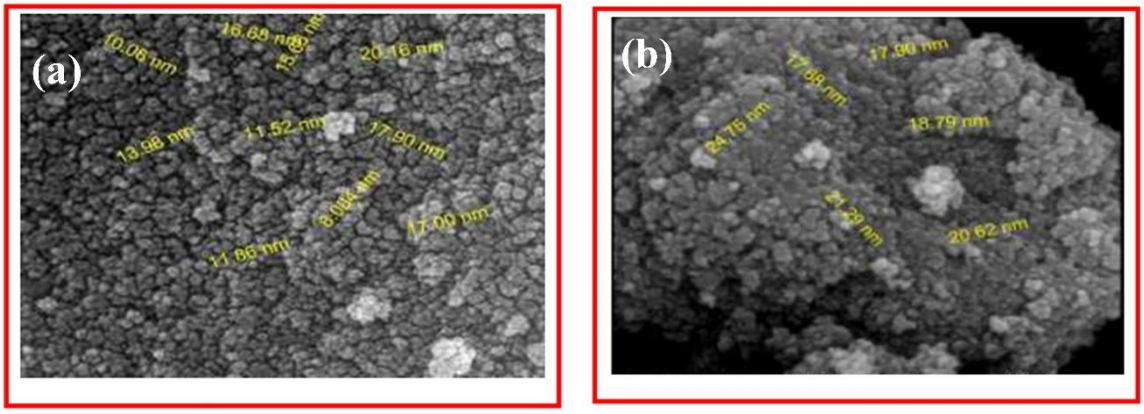

Fig. 7(a) SEM image of Iron oxide NPs and 7(b) SEM image of Chitosan modified Iron oxide NPs

3.8 Toxicity study

Fig 8(a-b) Growth kinetics of Bacillus subtilis in the presence of iron oxide nanoparticles and in the presence of Chitosan modified iron oxide nanoparticle and Fig 9(a-b) shows that the growth of the *E. coli* strains is hindered in the presence of iron oxide NPs and in the presence of Chitosan modified iron oxide nanoparticle. Yet, neither strain was affected by the presence of chitosan-modified iron oxide NPs. The phase contrast microscopic image of *E. coli* and *B. subtilis* is shown in Fig. 10 and 11 respectively. When bacteria come into contact with iron oxide NPs, they congregate, but when modified iron oxide NPs are present, there are no discernible differences. From the above graphs it is observed that in the presence of iron oxide nanoparticles growth of both Bacillus subtilis and E. coli strain is inhibited. Iron oxide nanoparticles show more antimicrobial activity to Bacillus subtilis than E. coli. The bacterial cells clump together when it comes in contact with the iron oxide nanoparticle where as there is no significant change in the presence of modified iron oxide nanoparticle.

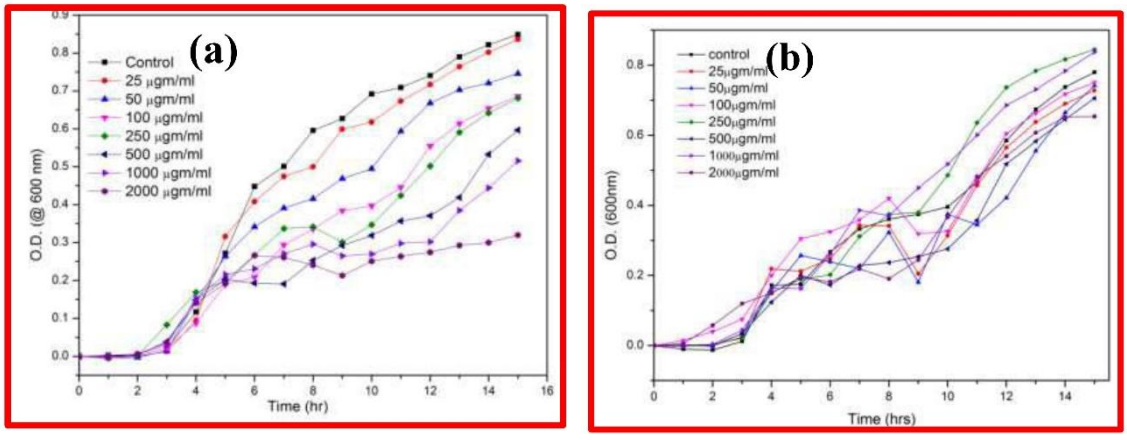

Fig 8(a) Growth kinetics of Bacillus subtilis in the presence of iron oxide nanoparticles (b) in the presence of Chitosan modified iron oxide nanoparticle

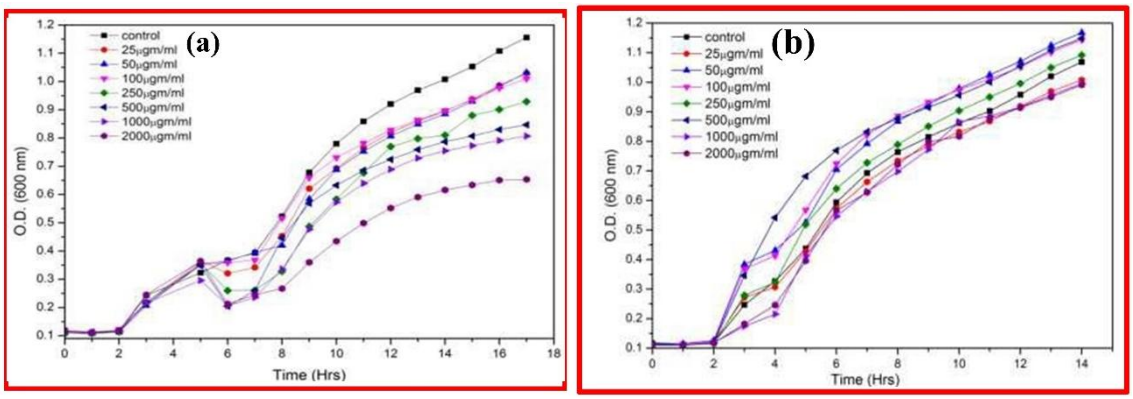

Fig. 9(a) Growth kinetics of *E. coli* in the presence of iron oxide NPs (b) in the presence of chitosan modified iron oxide NPs

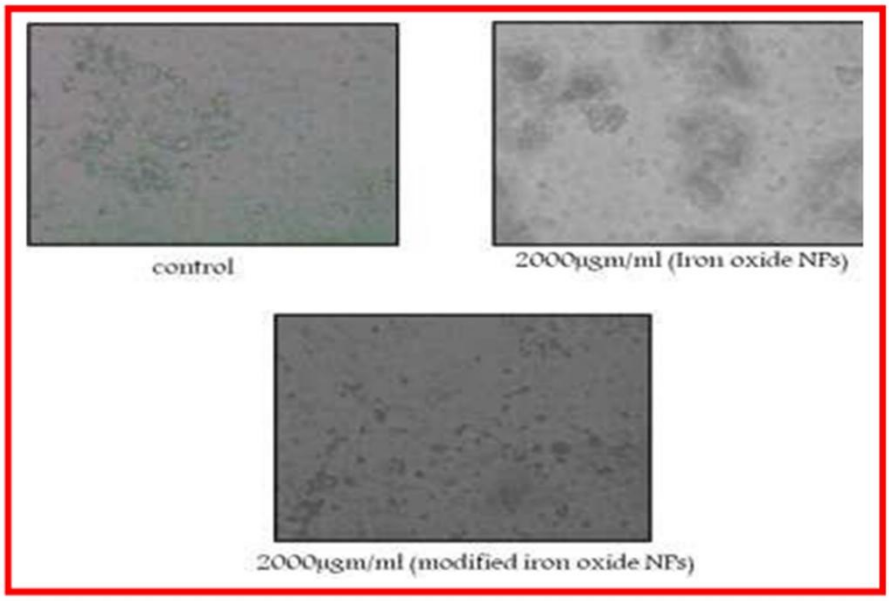

Fig. 10 Phase contrast microscopic image of *E. coli*

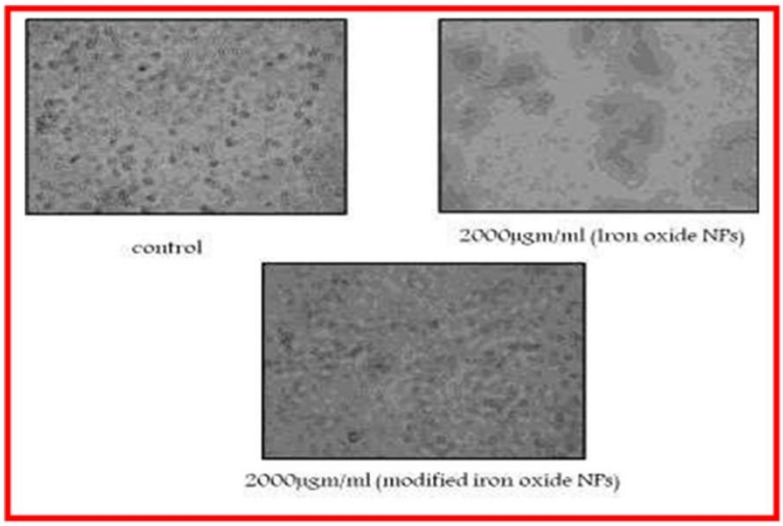

Fig. 11 Phase contrast microscopic image of *B. subtilis*

4 CONCLUSION

B. subtilis and *E. coli* were used as test organisms for studying the toxicity of iron oxide NPs and modified iron oxide NPs. It was concluded that iron oxide NPs have toxicity towards these test organisms at higher concentrations, whereas modified iron oxide NPs do not have this property. The research supports the idea that surface modification with biocompatible substances like chitosan can reduce the toxicity of NPs. Iron oxide NPs potentially inhibited the growth of test organisms- *B. subtilis* and *E. coli.* The results confirmed the toxicity effect of iron oxide NPs and non-toxicity of chitosan modified iron oxide NPs.

References

[1] Rathi, V. H, Jeice, A.R,(2023) Green fabrication of titanium dioxide nanoparticles and their applications in photocatalytic dye degradation and microbial activities, Chemical Physics Impact 6, 100197.

[2] Laurent, S., et al., (2008) Magnetic iron oxide nanoparticles: synthesis, stabilization vectorization, physicochemical characterizations, and biological applications. Chemical reviews, 108(6), 2064-2110.

[3] Rathi, V.H., Jeice, A.R.(2023) Green-fabrication of CuO nanoparticles using various plant extracts and their multifaceted applications in photocatalytic cationic dye

degradation and antimicrobial activities. Biomass Conv. Bioref. 12

[4] Prammitha R, Jeice. A. R, Jayakumar. K, (2023) , Influences of calcination temperature on titanium dioxide nanoparticles synthesized using *Averrhoa carambola* leaf extract: in vitro antimicrobial activity and UV-light catalyzed degradation of textile wastewater. Biomass Conv. Bioref. 12

[5] Faraji, M., Y. Yamini, and M. Rezaee, (2010) Magnetic nanoparticles: synthesis, stabilization, functionalization, characterization, and applications. Journal of the Iranian Chemical Society 7(1): p. 1-37.

[6] Prammitha R, Jeice. A. R, Jayakumar. K, (2023) Review of green synthesized TiO2 nanoparticles for diverse applications, Surfaces and Interfaces, 39,2023,102912

[7] Naqvi, S., et al., Concentration-dependent toxicity of iron oxide nanoparticles mediated by increased oxidative stress. Int J Nanomedicine. 5 983-989.

[8] Singh, R.P., et al., (2011) Biological approach of zinc oxide nanoparticles formation and its characterization. Adv. Mat. Lett. 2(4), 313-317

[9] Yang, W.J., et al., (2013) Difference between toxicities of iron oxide magnetic nanoparticles with various surface-functional groups against human normal fibroblasts and fibrosarcoma cells. Materials. 6(10) 4689-4706.

[10] Gordon, T., et al., (2011) Synthesis and characterization of zinc/iron oxide composite nanoparticles and their antibacterial properties. Colloids and Surfaces A: Physicochemical and Engineering Aspects. 374(1) 1-8.

[11] Kandpal, N.D, et al., (2014) Co-precipitation method of synthesis and characterization of ironoxide nanoparticles. Journal of Scientific & Industrial Research. 73(2): p. 87-90.

[12] Muthiah, M., I.-K. Park, and C.-S.Cho, (2014) Surface modification of iron oxide nanoparticles by biocompatible polymers for tissue imaging and targeting. Biotechnology Advances. 31(8): p. 1224-1236.

[13] Singh, N., etal., (2010) Potential toxicity of superparamagnetic iron oxide nanoparticle (SPION), Nano reviews. 1p.5358

[14] Thanh,V.M, Huong,N.H,, Nam,d.T, Dung,N.D.T, undefined Le Van Thu, Minh-Tri Nguyen-Le (2020) Synthesis of Ternary Fe_3O_4/ZnO/Chitosan Magnetic Nanoparticles via an Ultrasound-Assisted Coprecipitation Process for Antibacterial Applications, Journal of Nanomaterials, 2020, 1-9

[15] Li, G.-Y., et al., (2008) Preparation and properties of magnetic Fe_3O_4-chitosan nanoparticles. Journal of Alloys and Compounds, 466(1), 451- 456.

[16] Kim, E.H., Y. Ahn, and H.S. Lee, (2007) Biomedical applications of superparamagnetic iron oxide nanoparticles encapsulated within chitosan. Journal of

Alloys and Compounds, 434, 633-636.

[17] Dung, D.T.K., et al., Preparation and characterization of magnetic nanoparticles with chitosan coating. Journal of Physics: Conference Series.187 (2009) 012036

[18] Gupta, A.K. and M. Gupta, (2005) Synthesis and surface engineering of iron oxide nanoparticles for biomedical applications. Biomaterials, 26(18) 3995-4021.

[19] Laurent, S., et al., (2009) Magnetic Iron Oxide nanoparticles: Synthesis, Stabilization, Vectorization, Physicochemical Characterizations, and Biological Applications. Chemical reviews, 110(4) 2574-2574.

[20] Zhu, X., S. Tian, and Z. Cai, (2012) Toxicity assessment of iron oxide nanoparticles in zebrafish (Danio rerio) early life stages. Plos One. 7(9) 1-6